The dynamics of infragravity wave transformation over a fringing reef

Andrew Pomeroy,[1,2,3] Ryan Lowe,[1] Graham Symonds,[4] Ap Van Dongeren,[2] and Christine Moore[5]

Received 24 June 2012; revised 20 September 2012; accepted 21 September 2012; published 20 November 2012.

[1] A 3 week field study was conducted to investigate the dynamics of low-frequency (infragravity) wave motions over a fringing reef at Ningaloo Reef, Western Australia. Short-period wave motions (0.04–0.2 Hz) were observed to dissipate on the reef crest beyond which infragravity wave motions (0.004–0.04 Hz) gradually dominated toward the lagoon. However, both the short waves and the infragravity waves were relatively small (both <0.3 m) on the reef flat owing to the shallow water depth (<2 m). The results revealed that the surf zone generation of free infragravity wave motions on the steep (∼1:20) fore-reef slope was dominated by breakpoint forcing (as opposed to shoaling bound waves), which was also supported by detailed numerical simulations of the generation process. This is consistent with theory suggesting the efficiency of the breakpoint forcing mechanism should be high in this steep-slope regime. Shoreward propagating infragravity waves traveled across the reef but were damped by bottom friction dissipation; however, this was at a rate much smaller than experienced by the residual short waves. With these rates of frictional dissipation also strongly dependent on the water depth over the reef, the infragravity wave heights increased at higher water levels and hence were strongly modulated by the tide. Due to the strong dissipation of infragravity waves over this wide and shallow reef that is hydraulically rough, any seaward propagating infragravity waves that reflected at the shoreline were small, leading to the dominance of progressive (shoreward propagating) infragravity wave motions throughout the reef and lagoon.

Citation: Pomeroy, A., R. Lowe, G. Symonds, A. Van Dongeren, and C. Moore (2012), The dynamics of infragravity wave transformation over a fringing reef, *J. Geophys. Res.*, *117*, C11022, doi:10.1029/2012JC008310.

1. Introduction

[2] A coastal reef functions as a protective barrier that, through interactions between the offshore hydrodynamic forcing (e.g., swell waves, wind, and tides) and the specific morphology of the reef, determine the hydrodynamic processes (waves, currents and water levels) that occur within the nearshore zone [*Monismith*, 2007]. These nearshore processes have been identified to be important to many ecological processes within reef environments such as: the control of the spatial distribution of dissolved [*Atkinson and Falter*, 2003; *Zhang et al.*, 2011] and particulate [*Yahel et al.*, 1998; *Wyatt et al.*, 2010] nutrient uptake by reef organisms, ecological zonation [*Dollar*, 1982] and larval recruitment pathways [*Roberts*, 1997; *Kraines et al.*, 2001]. Furthermore, the physical presence of a reef shapes the nearshore sediment transport pathways [*Storlazzi et al.*, 2004], controls the associated long-term morphological changes to a coastline [*Sanderson*, 2000], and helps to buffer coasts from extreme forcing events such as hurricanes/cyclones and tsunamis [*Kunkel et al.*, 2006]. While the importance of some of these nearshore hydrodynamic processes to reef systems is well recognized, the detailed dynamics of many processes still remain poorly understood (certainly in comparison to analogous processes on sandy beach coasts).

[3] The influence of a reef's morphology on swell wave dissipation and associated wave-driven circulation has been the subject of a number of recent studies. This work has shown that the dynamics of swell wave breaking can differ significantly on steep fore-reef slopes relative to classic mild-slope sandy beaches [*Massel and Gourlay*, 2000; *Sheremet et al.*, 2011], with some wave energy (depending on the water depth) transmitted shoreward out of the surf zone to the reef flat. While wave breaking dissipation usually dominates in the vicinity of the surf zone, rates of bottom friction

[1]School of Earth and Environment and UWA Oceans Institute, University of Western Australia, Crawley, Western Australia, Australia.
[2]Department ZKS and Department HYE, Deltares, Delft, Netherlands.
[3]Section Hydraulic Engineering, Faculty of Civil Engineering and Geosciences, Delft University of Technology, Delft, Netherlands.
[4]Centre for Australian Weather and Climate Research, CSIRO Wealth from Oceans Flagship, Wembley, Western Australia, Australia.
[5]Department of Civil and Environmental Engineering, Stanford University, Stanford, California, USA.

Corresponding author: A. Pomeroy, School of Earth and Environment, University of Western Australia, Crawley, WA 6009, Australia. (andrew.pomeroy@uwa.edu.au)

0148-0227/12/2012JC008310

dissipation can be substantial (due to the large biogenic roughness of coral reefs) and often dominates over the reef flat once wave breaking becomes minimal [*Lowe et al.*, 2005]. Other studies have investigated the wave-driven currents within reefs, generated by wave forces (radiation stress gradients) arising from swell wave dissipation, with initial work focused on those reefs with atoll and barrier reef morphologies (both having large expansive lagoons) [e.g., *Munk and Sargent*, 1948; *Kraines et al.*, 1999]. More recent work has focused on the dynamics within fringing reef systems, where the reefs are separated from a coastal landmass by narrower, shallow lagoons [e.g., *Lowe et al.*, 2009; *Taebi et al.*, 2011; *Hoeke et al.*, 2011]. For these fringing reefs, the particular geometry of the lagoon and/or channels (gaps) in the reef have been shown to play a major role in the momentum balances established across reef-lagoon systems and ultimately the magnitude of the wave-driven flows and related coastal flushing rates [*Lowe et al.*, 2010].

[4] Therefore, while extensive research conducted over the past several decades has significantly improved our understanding of the transformation of short period swell waves (with peak periods of 5–25 s) and mean wave-driven currents within reefs, very little is presently known about the dynamics of low-frequency wave motions (also called infragravity or IG waves) within reef systems. IG wave motions (those with periods of 25 s to tens of minutes) have been studied thoroughly on sandy beaches for many decades, from which two mechanisms are known to generate IG waves in the nearshore zone.

[5] 1. IG waves in the form of (coupled) forced long waves that are generated by nonlinear interactions between incident (primary) sea/swell waves [*Longuet-Higgins and Stewart*, 1962]. These waves travel from deep water and, due to the continuous forcing of these waves by the shoaling primary short waves, are amplified over the sloping seabed in the nearshore zone up to the zone of initial breaking [e.g., *List*, 1992; *Masselink*, 1995] and possibly within the surf zone [*Foda and Mei*, 1981; *Schäffer and Svendsen*, 1988]. These waves are often referred to as bound long waves, which are thought to be "released" as free waves during short period wave breaking in the surf zone; note that in this study we will refer to these free waves as "shoaling bound waves" [*Battjes et al.*, 2004].

[6] 2. Alternatively, free IG waves may be generated within the surf zone of a sloping beach by the time-varying oscillation (excursion) of the short-wave breakpoint [*Symonds et al.*, 1982]. These IG waves are often referred to as "breakpoint-generated waves" [*Baldock*, 2012], which we will also use in this paper. While both types of free waves are likely to be generated on beaches, most studies on mild sloping beaches has indicated that IG wave energy tends to be the result of shoaling bound waves (mechanism 1) [*Herbers et al.*, 1995; *Masselink*, 1995; *Ruessink*, 1998; *Janssen et al.*, 2003]. However, the importance of surf zone generated waves (mechanism 2) is thought to significantly increase as the relative slope at the breakpoint increases, which implies that a transition exists between these two generation regimes based on the slope [*Battjes et al.*, 2004] (see also *Baldock* [2012] for a recent review).

[7] Once free IG waves propagate out of a surf zone toward shore, they may then reflect seaward at the shoreline (leading to a standing wave pattern in the cross-shore direction [e.g., *Munk*, 1949; *Tucker*, 1950; *Suhayda*, 1974], or may be trapped as alongshore-propagating edge waves [e.g., *Huntley et al.*, 1981]. Initial work, again focusing on sandy beaches, suggested frictional dissipation may play an important role in observed IG energy losses [*Henderson and Bowen*, 2002]. However, more recent work has suggested that much of these losses may instead be due to wave-wave (triad) interactions that transfer IG energy back to higher frequencies [*Henderson et al.*, 2006; *Thomson et al.*, 2006] or the breaking of the IG waves in shallow water [*Van Dongeren et al.*, 2007]. Overall, while IG waves have been very well described on sandy beach coasts (including processes from generation through to dissipation), the analogous dynamics of IG waves in reef systems have yet to be comprehensively studied and are likely to differ considerably due to the stark differences in bottom topography and roughness characteristics.

[8] IG waves have been recognized as being important on reefs for many years [e.g., *Hardy and Young*, 1996; *Lugo-Fernández et al.*, 1998; *Brander et al.*, 2004], with these observations (mostly descriptive) suggesting they may make an important contribution to the overall water motion within reef-lagoon systems. Recent work has also indicated that the amplitude of IG waves can be significantly enhanced during periods of resonance, when the time scale of the offshore forcing matches the resonant mode for the reef morphology, i.e., based on the observations by *Péquignet et al.* [2009] at Guam during a topical storm. Laboratory studies [*Nakaza and Hino*, 1991; *Demirbilek et al.*, 2007] utilizing physical reef models have also elucidated important infragravity processes such as the loss of IG wave energy due to nonlinear interactions (thus analogous to beaches); however, in these idealized laboratory and their related numerical modeling studies [*Nwogu and Demirbilek*, 2010; *Sheremet et al.*, 2011], a realistic bottom roughness was not considered (i.e., the reef prototypes had smooth plastic walls), which may not capture the complete field dynamics. Presently, major knowledge gaps still remain in our understanding of the IG wave dynamics operating within real coral reef systems. In this paper, we describe results from a 3 week field study that was designed to investigate the dynamics of IG waves across a fringing reef-lagoon system (Ningaloo Reef) in Western Australia. The objective of this study was to use the field data obtained on this reef to investigate how IG waves are generated on reefs, how they propagate, and how they ultimately lose their energy. We then apply an IG wave-resolving numerical model (XBeach) to supplement the field observations and provide further insight into the IG wave generation processes.

2. Methodology

2.1. Site Description

[9] The field experiment was conducted on an ~3 km section of Ningaloo Reef in Western Australia, near Sandy Bay (22°13′S, 113°49′E, Figure 1). At this site, the fore-reef slope rises at ~1:20 to the reef crest, which is located ~1.4 km from the coastline. The shallow reef flat, of between 1 m and 2 m deep and approximately 500 m in width, is covered by dense assemblages of tabular plate Acoropora coral (Figures 1b and 1c) [*Wyatt et al.*, 2010].

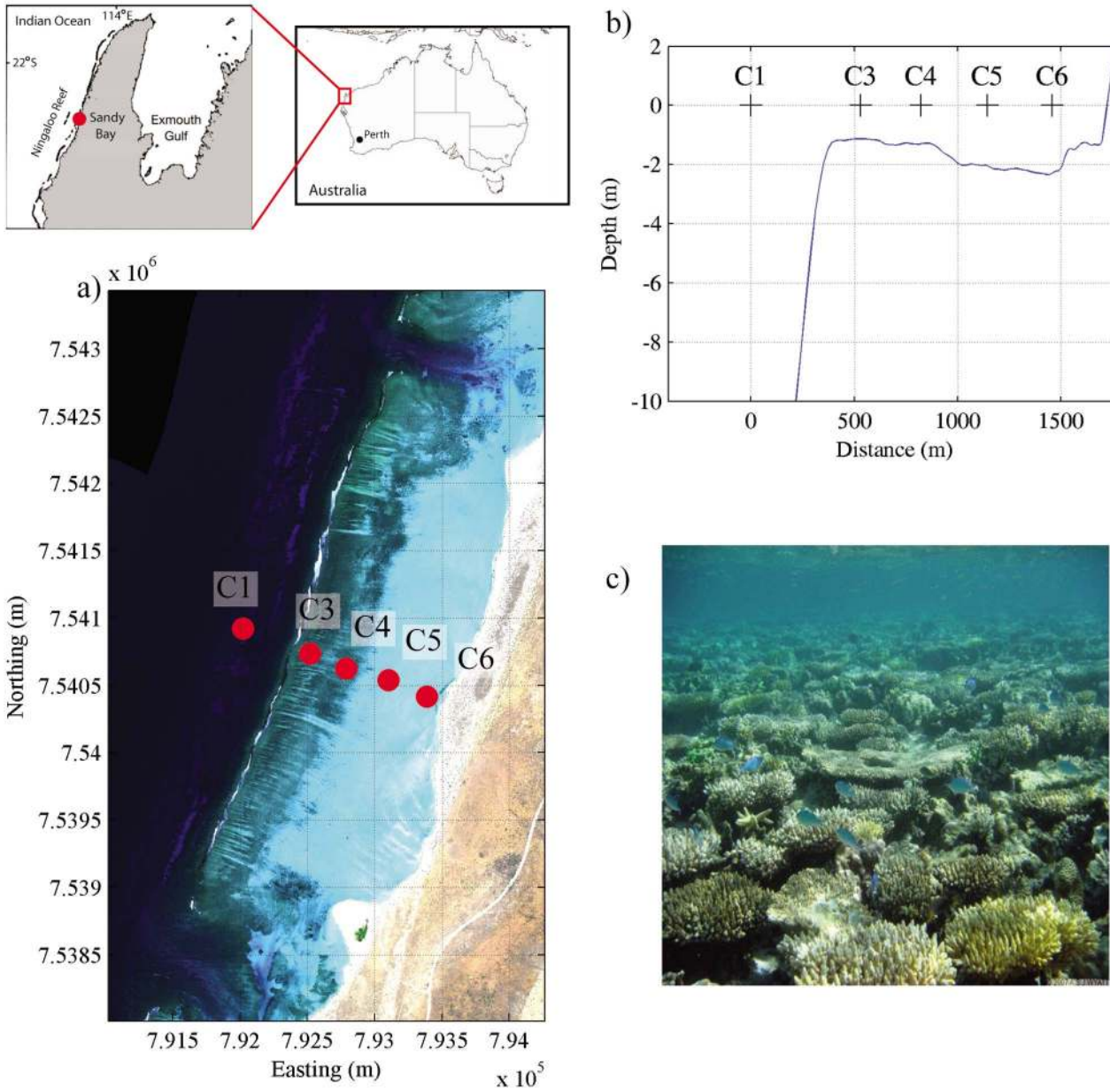

Figure 1. (a) Location of Sandy Bay (Ningaloo Reef) along the northwest coast of Australia with the instrument locations shown. (b) The bathymetry profile along the cross-shore instrument transect (C1–C6). (c) Photo of the reef bottom near site C3.

[10] A lagoon, ~850 m wide with an average depth of 2–3 m, separates the reef from the shore and primarily consists of patchy coral reef communities, sand and coral rubble. Depth-induced wave breaking drives a mean current field characterized by onshore flow over the reef crest causing wave setup in the lagoon [*Taebi et al.*, 2011]. This setup creates an alongshore pressure gradient in the lagoon that drives the flow toward gaps in the reef where the flow returns offshore. The morphology of this section of reef, as well as its benthic composition, is fairly typical of Ningaloo Reef as a whole [*Wyatt et al.*, 2010; *Taebi et al.*, 2011].

2.2. Field Experiment and Instrument Configuration

[11] A synchronous array of ten moored instruments was deployed for a period of three weeks during the austral winter of 2009 (9 June to 1 July). Five were deployed at sites along the reef flat parallel to the coastline and five were deployed along a cross-shore transect from offshore of the reef to near the shoreline. The results presented in this paper focus only on the cross-shore wave variability from the cross-shore transect (C1–C6) data of the field experiment (Figures 1a and 1b). Instrument package C2 was colocated with C1 (for redundancy) and hence does not provide additional

Table 1. Instrument Site Information and Sampling Configuration[a]

Site	Depth (m)	Instrument	Sampling Information
C1 (fore reef)	15.7	Nortek AWAC	1 Hz with 2048 s burst every 3600 s; pressure sample height: 0.5 m; velocity sample height: 10 m
C3 (reef flat)	1.79	Nortek Vector ADV	Continuous sampling at 2 Hz; pressure sample height: 0.1 m; velocity sample height: 0.5 m
C4 (reef flat)	1.49	Nortek Vector ADV	Continuous sampling at 2 Hz; pressure sample height: 0.1 m; velocity sample height: 0.5 m
C5 (lagoon)	1.61	Nortek Vector ADV	2 Hz continuously; pressure sample height: 0.1 m; velocity sample height: 0.5 m
C6 (lagoon)	1.26	Seabird SBE26	2 Hz with 2048 s burst every 7200 s; sample height: 0.1 m

[a]Sample heights are relative to the bed.

information so it has been excluded from the analysis. The remaining five instruments consisted of current meters/profilers recording 3-D velocities and pressure, including a 1 MHz Nortek AWAC recording velocities and sea surface elevation (via acoustic surface tracking, AST) located at C1, three Nortek Vector acoustic Doppler velocimeters (ADVs) located between C3 and C5 and a pressure-sensor wave gauge (Seabird SBE26) at C6. Table 1 summarizes the instrument locations and sampling configurations.

2.3. Data Analysis

2.3.1. Surface Elevation Time Series Analysis

[12] One-dimensional wave spectra $S_{\eta\eta}$ were estimated for each hourly burst of data by computing the spectral density of the water surface elevation fluctuations η measured directly by the AWAC AST, and for the other instruments, by conversion of the spectral density of the pressure fluctuations to surface elevation spectra. Linear wave theory was used to convert the shorter-period swell waves [*Dean and Dalrymple*, 1991] but was not needed for the longer period infragravity waves (i.e., these waves were shallow, even on the fore reef at C1). The spectra were computed using a Welch's averaged modified periodogram, with 50% overlap and Hanning windows applied, to reduce spectral leakage. Raw easterly and northerly components of the velocity time series were rotated into cross-shore U and alongshore V components based on the measured angle normal to both the reef crest and shore (positive direction $\sim$110° clockwise from north).

[13] A wave separation frequency (f_{split}), defined as half of the offshore peak frequency [*Roelvink and Stive*, 1989], was calculated for each burst of data. The mean f_{split} was $\sim$0.04 Hz and was located between the high- and low-frequency surface elevation peaks (see below). This value was thus used to separate the results into "short waves" (frequency 0.04–0.2 Hz or period 5–25 s) and infragravity waves (frequency 0.004–0.04 Hz or period 25–250 s) components. The upper, lower and separation frequencies used here are consistent with other nearshore studies [e.g., *Elgar et al.*, 1992; *Sheremet et al.*, 2002; *Péquignet et al.*, 2009]. From these wave spectra, the root mean squared (rms) wave heights for the short-wave and IG bands ($H_{rms,sw}$ and $H_{rms,IG}$, respectively) were computed.

[14] A lagged correlation analysis [*Bendat and Piersol*, 1986] was used to investigate the relationship between the short-wave envelope on the fore reef (C1) and the shoreward, seaward and total IG surface elevations separately at each instrument site, following the approach by *List* [1992], *Janssen et al.* [2003], and *Baldock* [2006]. The time-varying amplitude $A(t)$ of the short-wave envelope was estimated using the Hilbert transform operator, which was low-pass filtered to obtain a smoothly varying envelope [*Janssen et al.*, 2003]. IG surface elevation and velocity time series were derived from the total signal by band-pass filtering the raw data in frequency space using the IG band limits. The total IG surface elevation time series were then separated into shoreward η_{IG}^{+} and seaward η_{IG}^{-} signals using the *Guza et al.* [1984] decomposition approach. The shoreward and seaward propagation of the IG waves were assumed to be at the linear shallow water wave speed $\sqrt{gh}$. The cross correlations and cross spectra between the envelope and the IG waves at C1 and the IG waves on the reef (C3 and C4) and in the lagoon (C5) were also quantified. We note that presence of very high friction over the reef theoretically has the potential to reduce the linear shallow water wave speed according to [e.g., *Roelvink and Reniers*, 2012]:

$$c = \sqrt{gh}\frac{1}{\sqrt{1+\left(\frac{f_c U_{IG} T_{IG}}{8h}\right)^2}} \quad (1)$$

where U_{IG} and T_{IG} are representative wave orbital velocities and periods, respectively, for the IG waves propagating over the reef, h is the water depth and f_c is a bottom friction coefficient. For typical values observed on the reef of $U_{IG} \sim 0.1$ m s^{-1}, $T_{IG} \sim 100$ s, $h \sim 1$ m and $f_c \sim 0.06$ (see below), equation (1) predicts that the shallow water wave speed will be reduced by <1% and hence its influence on c is negligible.

2.3.2. Energy Fluxes and Balances

[15] The cross-shore energy densities ($E^{\pm}$) of the shoreward and seaward propagating waves (superscripts $\pm$ respectively) at frequency f and location x were estimated by analyzing the colocated velocity and surface elevation data in frequency space following equation (2) of *Sheremet et al.* [2002]. The cross-shore energy fluxes ($F^{\pm}(f,x) = E^{\pm}(f,x)\sqrt{gh}$) of the shoreward ($F^{+}$) and seaward ($F^{-}$) propagating waves were integrated over the short-wave and IG frequency bands to obtain the bulk short-wave ($F_{sw}^{\pm}$) and IG wave ($F_{IG}^{\pm}$) energy fluxes. We note that the raw velocity data (near-surface bin) recorded by the AWAC at C1 were much noisier than the ADV data resulting in spikes in the velocity records and consequently the IG energy fluxes at C1 (not shown). Therefore, the results shown below for $F_{IG}^{\pm}$ at C1 had an 8 h moving average applied to the hourly burst data. The reflection coefficients for each cross-shore location were calculated as $R_{IG}^2(x) = F_{IG}^{-}(x)/F_{IG}^{+}(x)$ [*Sheremet et al.*, 2002]. We note that

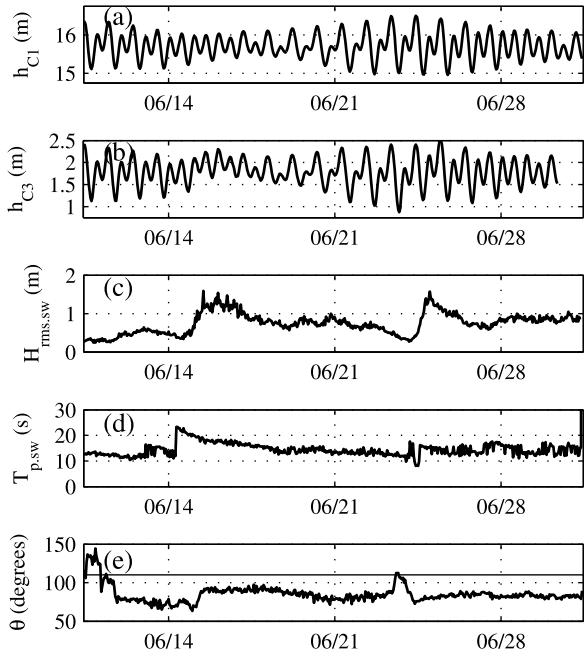

Figure 2. Water depth (a) on the fore reef at C1 and (b) on the reef flat at C3, along with the fore-reef (c) short-wave RMS wave height $H_{rms,sw}$, (d) peak wave period $T_{p,sw}$, and (e) mean wave direction θ, which were measured in the field experiment. The horizontal solid black line in Figure 2e denotes the shore normal direction (~110°).

applying the one-dimensional cross-shore energy balance equation is reasonable when the gradients in the net alongshore energy fluxes are small, i.e., when the ratio α defined in, e.g., *Henderson and Bowen* [2002] is small:

$$\alpha = \left|\frac{\partial F_{along}/\partial y}{\partial F_{cross}/\partial x}\right| \approx \frac{F_{along}L_{cross}}{F_{cross}L_{along}} \tag{2}$$

where F_{cross} and F_{along} are the net cross-shore and alongshore fluxes respectively, and L_{cross} and L_{along} are characteristic length scales over which the gradients (cross-shore and alongshore respectively) occur. On the reef flat where F_{cross}/F_{along} was typically >3 (not shown), and taking L_{cross} as the cross-shore width of the reef (~1.4 km) and L_{along} as the straight alongshore section of reef between the two channels (~6 km), this gives $\alpha \ll 1$.

[16] Rates of energy dissipation and losses within the IG wave band as the waves propagated across the reef were quantified for the reef flat region, shoreward of the surf zone (i.e., between sites C3 and C4) where short-wave breaking had ceased, using the cross-shore wave energy balance equation [e.g., *Henderson et al.*, 2006]:

$$\frac{\partial F_{IG}^{+}}{\partial x} = N_{IG} + D_{IG} \tag{3}$$

where N_{IG} describes possible nonlinear transfers of energy at IG frequencies due to wave-wave (triad) interactions and D_{IG} is the dissipation of IG wave energy by bottom friction. The nonlinear contribution to the total cross-shore energy flux [e.g., *Henderson et al.*, 2006] was calculated and found to have a mean contribution of ~5% and a maximum contribution of ~15% (not shown). The linear energy flux contribution was thus overwhelmingly dominant over the relatively shallow reef flat, likely due to the attenuation of IG wave heights over the reef by bottom friction, hence reducing their steepness. We therefore based the subsequent data analysis on the computed linear fluxes [e.g., *Sheremet et al.*, 2002]. The rates of nonlinear energy transfer N_{IG} between the IG waves and the higher-frequency waves were estimated as [e.g., *Herbers and Burton*, 1997]:

$$N_{IG} = \int_{0.004}^{0.04}\left(\frac{3\pi f}{h}\int_{-\infty}^{\infty}\mathrm{Im}[B(f',f-f')]df'\right)df \tag{4}$$

where B is the bispectrum constructed from the surface elevation signal [e.g., *Kim and Powers*, 1979; *Elgar and Guza*, 1985], which is integrated over the frequency pairs $(f', f-f')$ to determine the difference interaction between the IG frequency (f) and short-wave frequency (f'). We note that equation (4) was derived using "WKBJ" wave theory with a mild-slope approximation [see *Henderson et al.*, 2006], which is reasonable on the effectively flat reef section between C3 and C4 (Figure 1b). To attain statistical reliability in the bispectrum, a moving 3 h sample of data was evaluated using 1024 sample ensembles with 75% overlap. This resulted in a frequency resolution of 0.0015 Hz with ~39 degrees of freedom (dof).

[17] Rates of frictional dissipation within the infragravity band D_{IG} were estimated based on the residual energy flux ($D_{IG} = \partial F_{IG}^{+}/\partial x - N_{IG}$) per equation (3). These dissipation rates were then related to an empirical bottom friction coefficient (f_c) experienced by the IG waves defined according to a bottom friction formulation [e.g., *Henderson and Bowen*, 2002; *Van Dongeren et al.*, 2007]:

$$D_{IG} = f_c\left(\frac{g}{h^3}\right)^{1/2}\frac{H_{rms}}{\sqrt{8}}\frac{H_{rms,IG}^2}{8} \tag{5}$$

where H_{rms} is the total root-mean-square wave height and $H_{rms,IG}$ is the root-mean-square wave height for the infragravity band only.

3. Results

3.1. Wave Observations

[18] During the experiment, the incident short-wave heights $H_{rms,sw}$ measured offshore on the fore reef at C1 ranged from 0.24 m to 1.60 m, with a mean (μ) height of 0.74 m and a standard deviation (σ) of 0.27 m (Figure 2c and Table 2). These waves had peak periods (T_p) ranging from ~10 s to greater than ~23 s (Figure 2d), thus dominated by

Table 2. Summary of Wave Height Statistics for the Entire Experiment[a]

	$H_{rms,sw}$ (cm)		$H_{rms,IG}$ (cm)	
	μ	σ	μ	σ
C1	73.99	26.90	5.22	2.56
C3	8.47	4.60	8.81	4.79
C4	3.00	1.95	5.21	3.32
C5	2.40	1.57	4.88	2.85
C6	2.93	1.88	5.00	2.85

[a]Here μ and σ refer to the mean and standard deviation values.

swell, and generally approached the reef at an angle of between 70° and 100° (only 40° to 10° off the cross-reef direction, ~110°, Figure 2e). A large reduction in the short-wave heights (and hence short-wave energy) was observed on the reef flat near the crest at C3 (Figures 3a and 3c), located just shoreward of the surf zone. Further toward the shore, on the back of the reef flat (C4) and inside the lagoon (C5), the short-wave heights decreased substantially, i.e., $H_{rms,sw}$ at C5 was reduced by 70% from values at C3 (Figures 3e and 3g). Notably, the short-wave heights measured at sites on the reef flat located shoreward of the surf zone (i.e., C3–C5) were strongly modulated by changes in the tidal depth over the reef, due to tidal variations to the depth-limited wave height [*Hardy and Young*, 1996]. A summary of the wave statistics (mean and standard deviation over the experiment) at each site is provided in Table 2.

[19] The IG wave heights $H_{rms,IG}$ on the fore reef at C1 were considerably smaller (range: 0.01–0.18 m, μ = 0.05 m, σ = 0.03 m) than the corresponding short-wave heights (Figure 3a). The wave spectra (Figure 3b) also show very little energy within the IG frequency band, with the exception of the period 14–19 June, when the incident short-wave heights were relatively large. Values of $H_{rms,IG}$ were slightly higher on the reef crest (C3) than on the fore reef (Figure 3c) and gradually decayed as they propagated over the reef flat toward the back reef (C4) and to the lagoon (C5), albeit at a much slower rate than the short waves (Figures 3e and 3g). These differences in the rates of wave attenuation between the short and IG waves result in the IG waves becoming increasingly important across the reef until they eventually dominate over the short waves. The dominance of the IG waves on the back reef and in the lagoon (C4 and C5) is clearly visible in the wave spectra (Figures 3f and 3h). The IG wave heights for sites on the reef (C3–C5) were also tidally modulated and in phase with the short-wave height variations, i.e., an increase in the tidal depth led to higher IG waves over the reef.

[20] On the fore reef (C1), the ratio $H_{rms,IG}/H_{rms,sw}$ showed little variability with tidal depth h measured on the reef at C3, i.e., this ratio was roughly constant at 8% (Figure 4a). Note that in this study h represents the total water depth, which may arise from both tidal and wave setup variations. On the reef flat and in the lagoon (Figures 4b and 4c), however, the ratio $H_{rms,IG}/H_{rms,sw}$ (here again normalized by the incident swell height at C1) responded strongly to changes in the tidal depth h, reaching values as high at 15% near the reef crest when the tide was high (~2 m at C3). The results also indicate that during periods of low tide (i.e., when the depth measured at C3 was <1.2 m), the ratio ($H_{rms,IG}/H_{rms,sw}$) within the reef and lagoon was effectively zero (Figures 4b and 4c).

3.2. Generation and Propagation of Infragravity Waves

[21] The cross correlation of the measured short-wave envelope $|A(t)|$ at C1 (on the fore reef) with the local IG wave time series η_{IG} on the fore reef (C1), the reef flat (C3, C4) and in the lagoon (C5) were first calculated (Figure 5a) for a specific 1 h burst of data when the offshore wave height and the IG wave response were large (i.e., 16 June, 05:00). On the fore reef, a negative correlation peak ($R \sim -0.4$) occurred at near zero lag (Table 3), i.e., consistent with there being minimal lag between the short-wave envelope and a theoretical 180° out of phase bound long wave. On the reef crest (C3), a relatively strong positive correlation ($R \sim +0.6$) bounded by weaker negative correlations was present at 64 s lag. This correlation pattern persisted with increasing lags of 135 s and 209 s at C4 and C5, respectively. When averaging the individual cross-correlation results over the entire experiment (three weeks), a similar pattern of cross correlation between the short-wave envelope $|A(t)|$ at C1 and the IG wave time series η_{IG} were observed at all sites across the reef transect (Figure 5b). On Figures 5a we have superimposed the propagation times of a shallow water wave originating from C1 to the reef-lagoon sites that incorporates the cross-shore bathymetry profile (these theoretical lag times are also compared in Table 3). This change in correlation (negative offshore to positive nearshore) that tracks the theoretical propagation speed lends support to the idea that IG energy is generated between sensors C1 and C3, and hence dominantly by the moving breakpoint generation mechanism rather than by the shoaling bound wave [e.g., *Baldock*, 2006; *Lara et al.*, 2011]. However, this field data alone may arguably not provide conclusive evidence of the relative importance of each generation mechanism, due to the absence of instruments in the surf zone (between C1 and C3). Therefore, in section 4.2 we supplement this analysis with some targeted numerical modeling to further confirm the generation mechanism.

[22] Finally, in Figure 5c we show the computed phase spectrum from a cross-spectral analysis of η_{IG} between C3 and C4 for the wave burst (16 June, 05:00), and observe the classic linear phase ramps associated with a dominant shoreward propagating progressive waves. These dynamics are consistent with the time domain results in Figure 5a, where no significant seaward propagating IG signal is observed over the reef that is required to support a standing wave pattern.

3.3. Energy Fluxes, Nonlinear Energy Transfer, and Dissipation

[23] On the fore reef (C1), the cross-shore short-wave fluxes F_{sw} were dominated by the shoreward component of the decomposed short-wave energy flux (Figure 6a) while the shoreward and seaward components of the IG fluxes F_{IG} were comparable, albeit the shoreward fluxes were slightly higher by a factor 1–2 (equivalent to $R^2_{IG} \sim 0.5$–1; Figures 6b and 6c). Near the reef crest (C3), there was a large reduction in the short-wave energy flux (relative to C1) by more than 2 orders of magnitude, due to wave breaking in the surf zone (Figures 6a and 6d). Conversely, at C3 the shoreward IG fluxes F^+_{IG} were comparable to C1, but the net shoreward energy flux ($F^+_{IG} - F^-_{IG}$) was much higher than at C1, thus consistent with the low R^2_{IG} values (typically <0.25; Figures 6e and 6f). These results are also consistent with the dominantly shoreward propagation of the IG wave signals observed in the cross-correlation analysis above. At C3, the shoreward short-wave signal showed a strong tidal modulation, whereas the shoreward IG fluxes were more weakly (but still) tidally modulated.

[24] On the back of the reef flat (C4), both the shoreward short-wave and IG fluxes were reduced (Figures 6g and 6h) relative to C3. However, the IG fluxes became greater than the short-wave flux at this location, with the shoreward

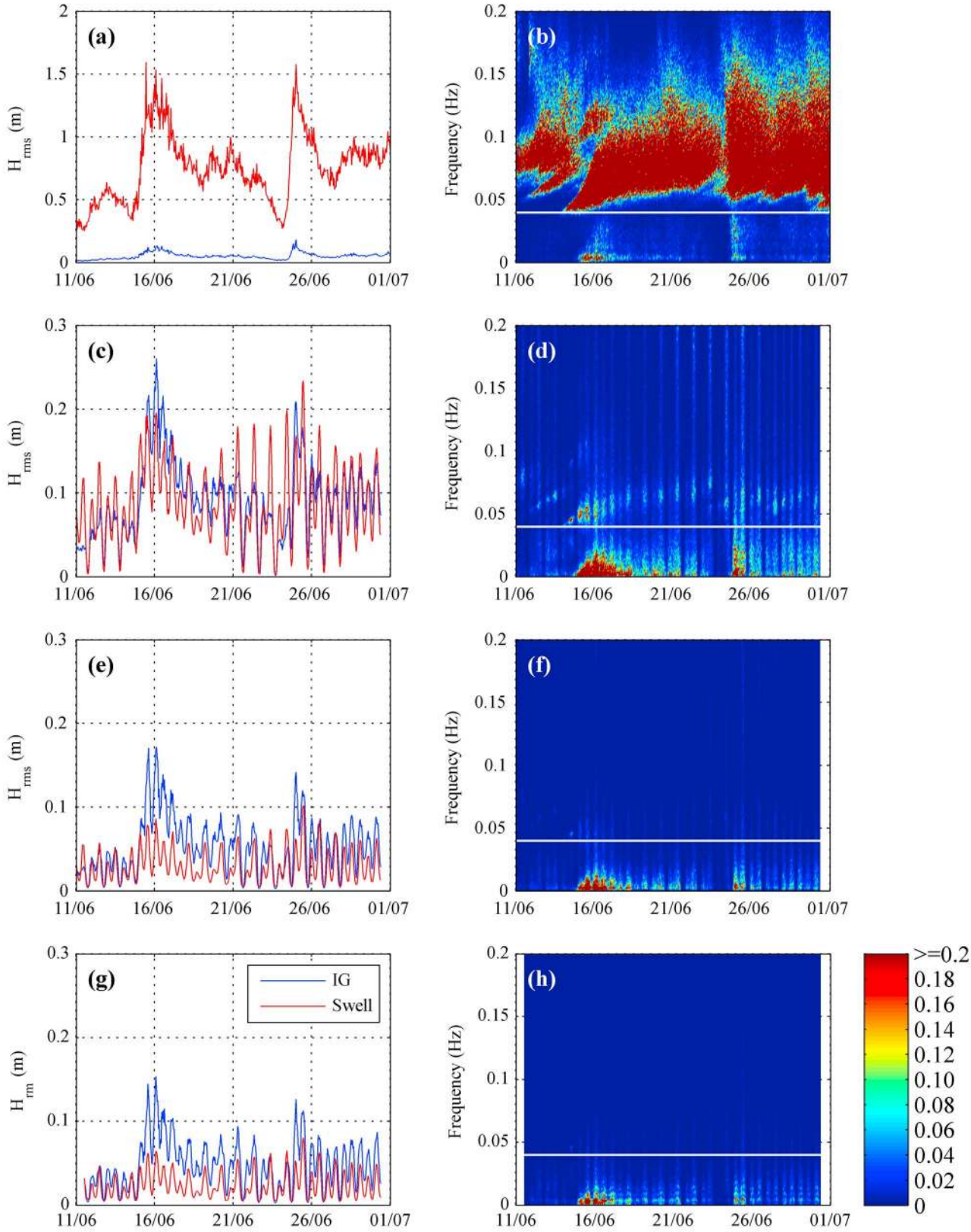

Figure 3. The burst-averaged short-wave and IG root-mean-square wave heights and wave spectra for sites (a, b) C1 (c, d) C3 (e, f) C4, and (g, h) C5. The energy density is represented by the color bar (m^2/Hz), and the resolution of the spectra is 0.001 Hz. The horizontal white line denotes the separation frequency (f_{split} = 0.04 Hz) separating the short-wave and infragravity bands.

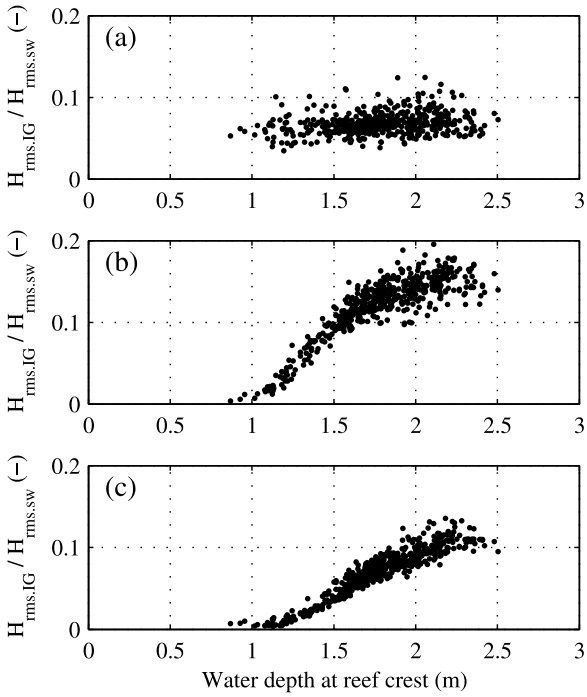

Figure 4. The IG wave height $H_{rms,IG}$ at (a) C1, (b) C3, and (c) C4, normalized by the fore-reef (C1) short-wave height $H_{rms,sw}$ and plotted as a function of the reef crest (C3) water depth h.

fluxes continuing to dominate over the seaward fluxes in both frequency bands (i.e., R^2_{IG} was typically 0.25–0.5; Figure 6i). In the lagoon at C5 (Figures 6j–6l) similar trends were observed, with the short-wave fluxes becoming negligible relative to the IG fluxes, and the seaward IG fluxes becoming a slightly more important fraction of the (still) dominant shoreward IG fluxes (R^2_{IG} typically ~0.5).

[25] The importance of nonlinear energy transfers and dissipation to the cross-shore IG wave energy balance was investigated. The analysis focused on the reef flat region (between C3 and C4), located shoreward of the surf zone, where negligible short-wave breaking occurs. The IG energy flux gradient dF^+_{IG}/dx between C3 and C4 was consistently negative throughout the experiment and thus represented a loss of energy from the IG frequency band (Figure 7a). Throughout much of the experiment -0.2 cm^2 s^{-1} < $dF^+_{IG}/dx < 0$ cm^2 s^{-1} except during the two larger short-wave events when $dF^+_{IG}/dx < -0.4$ cm^2 s^{-1}. This indicates that during the large short-wave conditions, the relatively large IG energy flux incident to the reef was dissipated on the reef flat between C3 and C4. The nonlinear energy transfer rate N_{IG} calculated at C3 was larger in magnitude than at C4 (Figure 7b) and, in contrast to the energy flux gradient measured between C3 and C4, N_{IG} was generally weakly positive at both locations (i.e., representing some small transfer of energy from the short-wave frequency band to the IG frequency band). The nonlinear energy transfer term was generally consistent throughout the experiment (nearly zero) with the exception of three periods: a small negative peak on 15 June, 10:00–13:00 and two positive peaks on 16 June, 12:00–15:00 and 24 June, 21:00–00:00. The absolute ratio

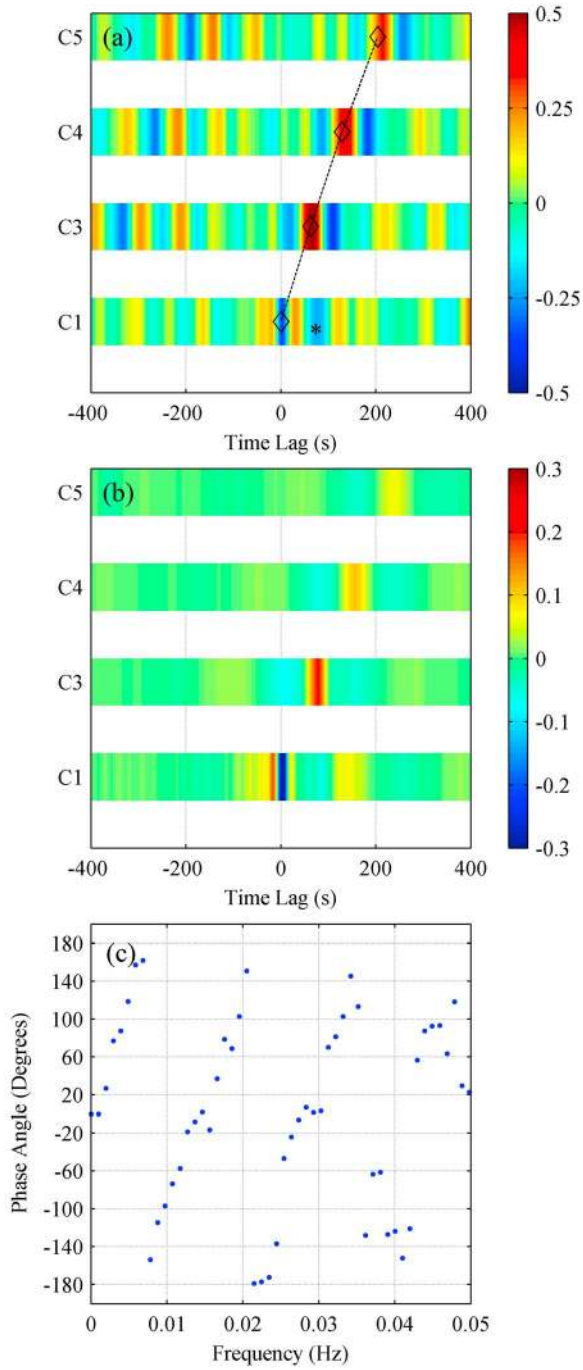

Figure 5. (a) Cross correlations for 16 June, 05:00, between the amplitude of the short-wave envelope $|A(t)|$ at C1 with the shoreward IG wave time series η_{IG} at each instrument location. The dotted line denotes the theoretical linear shallow water speed trajectory obtained by integration of the bathymetry profile. The star denotes the signature of a seaward propagating breakpoint generated IG wave (see section 4.2). (b) The mean (experiment averaged) of the individual cross correlations for all hourly bursts. (c) Phase angle and frequency relationship from cross-spectral analysis of η_{IG} between C3 and C4 for 16 June, 05:00.

Table 3. Observed Maximum Correlations *R* and Time Lag Times Compared With the Theoretical Lag Time[a]

Site	Observed		Theoretical Time Lag (s)
	R	Time Lag (s)	
C1 (fore reef)	−0.36	3 ± 4	0
C3 (reef flat)	+0.55	66 ± 7	62
C4 (reef flat)	+0.43	137 ± 8	129
C5 (lagoon)	+0.33	214 ± 8	204

[a]Uncertainties in the lag times reflect uncertainties in the width of the correlation versus lag peak.

(Figure 7c) of the nonlinear transfer term on the reef flat to the measured flux gradient at C3 was consistently less than 5%, except during the two large offshore swell events where the ratio became as high as 15%. This ratio was considerably less at the back of the reef flat (C4).

[26] The time series of IG wave bottom friction dissipation rates over the reef flat D_{IG} were used with equation (5) to compute values of the bottom friction coefficient f_c associated with the observed IG wave decay (Figure 8). The mean f_c for the entire experiment was 0.06 (σ = 0.02) (Figure 8a). Some scatter in f_c arose from changes in the tidal depth h over the reef (Figure 8b), with f_c decreasing weakly as the depth (mean of C3 and C4) increased from 1 m to 2 m, albeit with significant scatter for depths <1 m.

4. Discussion

4.1. Observations of IG Wave Generation

[27] The observed change in the phase relationship from the cross-correlation analysis between the offshore short-wave envelope and the IG wave motions on the fore reef, reef flat and in the lagoon, suggested that the IG waves observed on the reef were dominantly generated by radiation stress forcing in the surf zone (i.e., via the breakpoint forcing mechanism) within statistical certainty (Table 3). In contrast, the much higher resolved cross-shore laboratory measurements of a mild-slope (∼1:70) beach prototype by *Janssen et al.* [2003] have shown that the negative correlation between the wave envelope and the IG waves (characteristic of a shoaling bound wave) propagated unaltered through the surf zone toward shore, thus suggestive of the more dominant role of shoaling bound waves to the IG waves generated in this system. *Baldock* [2006] conducted a similar cross-shore correlation analysis with laboratory measurements on a much steeper 1:10 beach (hence with a slope more similar to a reef) and observed the opposite phasing to *Janssen et al.* [2003], with a shift to a positive correlation near the surf zone, which he argued was consistent with the dominance of breakpoint forcing on this steep beach. Our observations are thus more similar to those of *Baldock* [2006].

[28] The importance of surf zone (breakpoint) forcing to IG wave generation was shown to depend on a normalized surf zone width parameter χ defined as [*Symonds et al.*, 1982]

$$\chi \equiv \frac{4\pi^2 h_b}{g T_{IG}^2 h_x^2} \tag{6}$$

where T_{IG} is the wave group period, h_b is the depth at the mean breakpoint position and h_x is the bottom slope. Based on typical values for this site ($T_{IG} \sim 100$ s, $h_b \sim 1$ m, $h_x \sim 1{:}20$) this results in $\chi \approx 0.16$ and is well within the range where breakpoint generation is thought to become effective (i.e., when $\chi < 10$) [*Battjes et al.*, 2004]. Note that *Symonds et al.* [1982] assumed a plane sloping beach to the shoreline to estimate the amplitude of the reflected IG wave as a function of χ, which does not hold in this case. Recently, *Baldock* [2012] proposed a modified surf zone parameter ξ to distinguish the importance of the two different IG generation regimes, which functionally depends on χ but also incorporates the role of the short-wave steepness, i.e.,

$$\xi \equiv \chi^{-1/2} \left(\frac{H_{o,sw}}{L_{o,sw}} \right)^{1/2} \tag{7}$$

where $H_{o,sw}/L_{o,sw}$ is the offshore (deep water) short-wave steepness. Based on a typical wave steepness at the study site ($H_{o,sw}/L_{o,sw} \sim 0.1$), this results in $\xi \approx 0.8$, which is far greater than has been observed on other sites [see *Baldock*, 2012, Table 1], including the steep beach study of *Baldock et al.* [2000] where values of ξ were up to ≈0.2; this strongly suggests that IG waves should be dominantly generated by the breakpoint forcing mechanism at this reef study site.

4.2. Numerical Experiments of Infragravity Wave Generation

[29] Finally, to provide more detailed insight into the IG generation process within the narrow surf zone (where no direct measurements were available) we supplemented the field analysis with one-dimensional (cross-shore) numerical experiments using the model XBeach [*Roelvink et al.*, 2009]. This targeted modeling was designed to isolate the importance of each generation mechanism under both an idealized (i.e., bichromatic wave group) and a realistic (i.e., irregular wave group) forcing condition. We note that a comprehensive modeling study of the full range of hydrodynamic processes (including mean wave-driven currents) on this section of reef during the study period, with a hindcast validation for both 1-D and 2-D model configurations, is reported elsewhere (A. Van Dongeren et al., Numerical modeling of low-frequency wave dynamics over a fringing coral reef, submitted to *Coastal Engineering*, 2012). However, in the present study we only apply the model under these two forcing scenarios, and utilize the much more highly spatially resolved model output to explore the IG wave dynamics in regions where no field data was available (e.g., within the surf zone) to provide further insight into the generation processes.

[30] XBeach is a two-dimensional time domain horizontal morphodynamic model. In the present application it is run in one-dimensional hydrodynamic mode (no morphological change). The model solves for the steady and unsteady (IG) surface elevation and particle velocities from the nonlinear shallow water equations of mass and momentum with radiation stress forcing. This forcing is calculated from the wave action equation for the time variation of the short-wave envelope on the wave group scale (i.e., the model does not resolve the shape of the short-wave motions themselves). The underlying assumption is that the short-wave energy propagates at the group speed when the spectra are narrow banded, which careful lab experiments [e.g., *Janssen et al.*, 2003] have confirmed and is also the case here. This forcing on the wave group scale generates IG wave motions

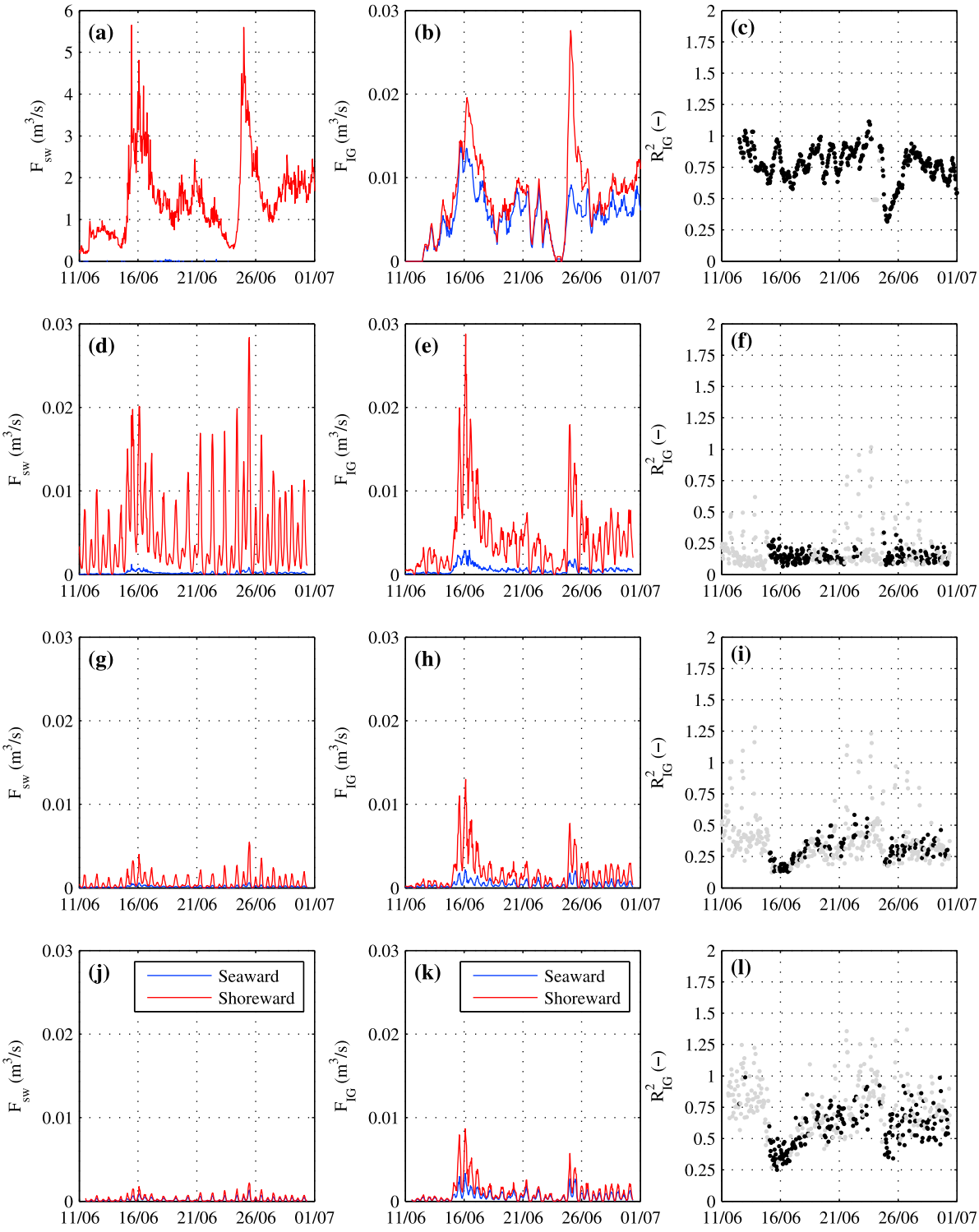

Figure 6. (left) The energy flux for short-wave frequencies for (middle) IG frequencies and (right) the ratio of the seaward and shoreward IG frequency band flux (reflection coefficients). (a–c) Instrument C1, (d–f) instrument C3, (g–i) instrument C4, and (j–l) instrument C5. The gray reflection coefficient points indicate when the seaward flux was below the estimated measurement noise floor ($F_{IG} < 0.0005$ m^3/s).

through offshore forcing and generation inside the surf zone (which includes breakpoint generation). We refer to *Roelvink et al.* [2009] and *Van Thiel de Vries* [2009] for details on model-data validation of the hydrodynamic model, as well as *Van Dongeren et al.* [2003] which demonstrated IG wave generation with a similar type model. XBeach requires input of the initial bathymetry and boundary conditions which are generated from offshore (measured or computed) wave

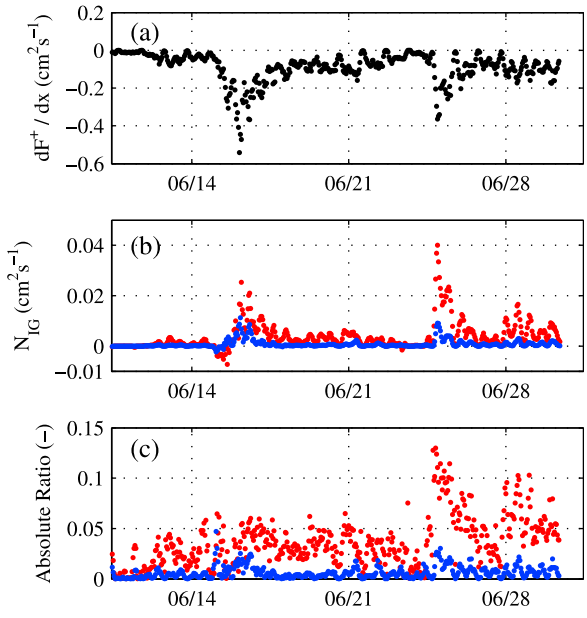

Figure 7. (a) Energy flux gradient over the reef flat (C3–C4). (b) Nonlinear energy transfer term at C3 (red) and C4 (blue). (c) Ratio (absolute value) of the nonlinear energy transfer term at C3 (red) and C4 (blue) with the energy flux gradient over the reef flat.

spectra (for the wave action equation and time-varying IG motions) and slowly varying (tidal) water levels from measurements or an outer domain model. We refer to *Van Dongeren et al.* [2003] for details on the boundary condition implementation. The model incorporated bathymetry for Ningaloo Reef, derived from high-resolution hyperspectral imagery (3.5 m horizontal resolution, <10% RMS depth error) [see *Taebi et al.*, 2011], and was configured with a spatially varying grid resolution ranging from 50 m offshore to as fine as ∼17 m in the surf zone region and over the reef. We finally note that both linear and nonlinear models, while derived based on mild slope assumptions, have frequently been applied successfully to relatively steep slopes in the literature, even to slopes of 1:5 [e.g., *Williams et al.*, 2012]. The Ningaloo fore-reef slope of ∼1:20 falls within the range of a steep beach [*Baldock*, 2012]; however, we recognize that the Ningaloo slope is much milder than many other reefs described in the literature where slopes approach near vertical [e.g., *Gourlay*, 1994].

[31] We first considered an idealized forcing case in which the reef was subjected to a bichromatic wave group (i.e., a single infragravity wave frequency). This model had open (weakly absorbing) boundaries on the offshore and onshore boundaries and bottom friction associated with the low-frequency waves was turned off (i.e., f_c = 0). The model results show that offshore of the surf zone ($x \lesssim 0$ m), the IG waves are small in height and display a standing wave pattern (i.e., a summation of seaward and shoreward propagating IG waves) with associated nodes and antinodes (Figure 9b). However, on the reef ($x \gtrsim 300$ m), the height of the shoreward propagating IG waves increase markedly, which is maintained across the reef flat and into the lagoon (as there is no frictional dissipation in this case). The waves propagate through the onshore boundary without reflection. To isolate if the increase in IG wave height is due to breakpoint generation of these waves or due to a shoaling bound wave, we ran a second simulation where the bound wave forcing was turned off in XBeach for a region extending from the offshore boundary to the surf zone, and also no bound wave was imposed on the offshore boundary (i.e., no IG wave generation for x < 30 m; Figure 9c). For this scenario, the small amplitude IG waves continue to be observed offshore of the reef crest and travel away from the reef with time, consistent with these waves being generated in the surf zone. The IG waves on the reef at C3 have effectively the same height (only 5% lower; see Table 4) than the results with the full forcing (i.e., with incident bound waves included). This indicates that the bulk of the IG wave energy observed on the reef is generated in the surf zone via breakpoint forcing, with only a small contribution from shoaling bound waves. Finally, we conducted a third scenario where we turned off surf zone forcing (within the region 30 m < x < 1410 m) but included the bound wave forcing (Figure 9d). The results show that without surf zone (breakpoint) forcing the IG waves on the reef are minimal (reduced by ∼80%; see Table 4).

[32] We also conducted realistic field case simulations with irregular wave forcing using the conditions observed during a swell peak (16 June 05:00), and with bottom friction turned on (f_c = 0.06) and applied uniformly throughout the model domain. Figure 9a shows that the XBeach model accurately reproduces the spatial trends in both the short-wave $H_{rms,sw}$ and IG wave $H_{rms,IG}$ heights, including the strong decay in the short waves and increase in IG waves within the surf zone (between C1 and C3), as well as the decay in the IG wave heights across the reef by bottom friction. Inspection of the time series results with full forcing

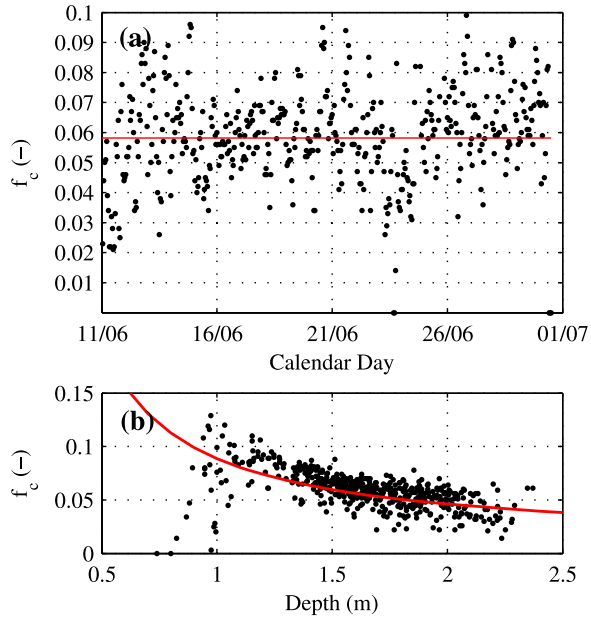

Figure 8. Estimated bed friction coefficient f_c computed for each burst of data plotted as a function of (a) time and (b) mean water depth (recorded at C3). The red line in Figure 8a indicates the mean value f_c = 0.06. The red line in Figure 8b shows the f_c versus depth relationship predicted by equation (8) with z_0 = 0.15 m.

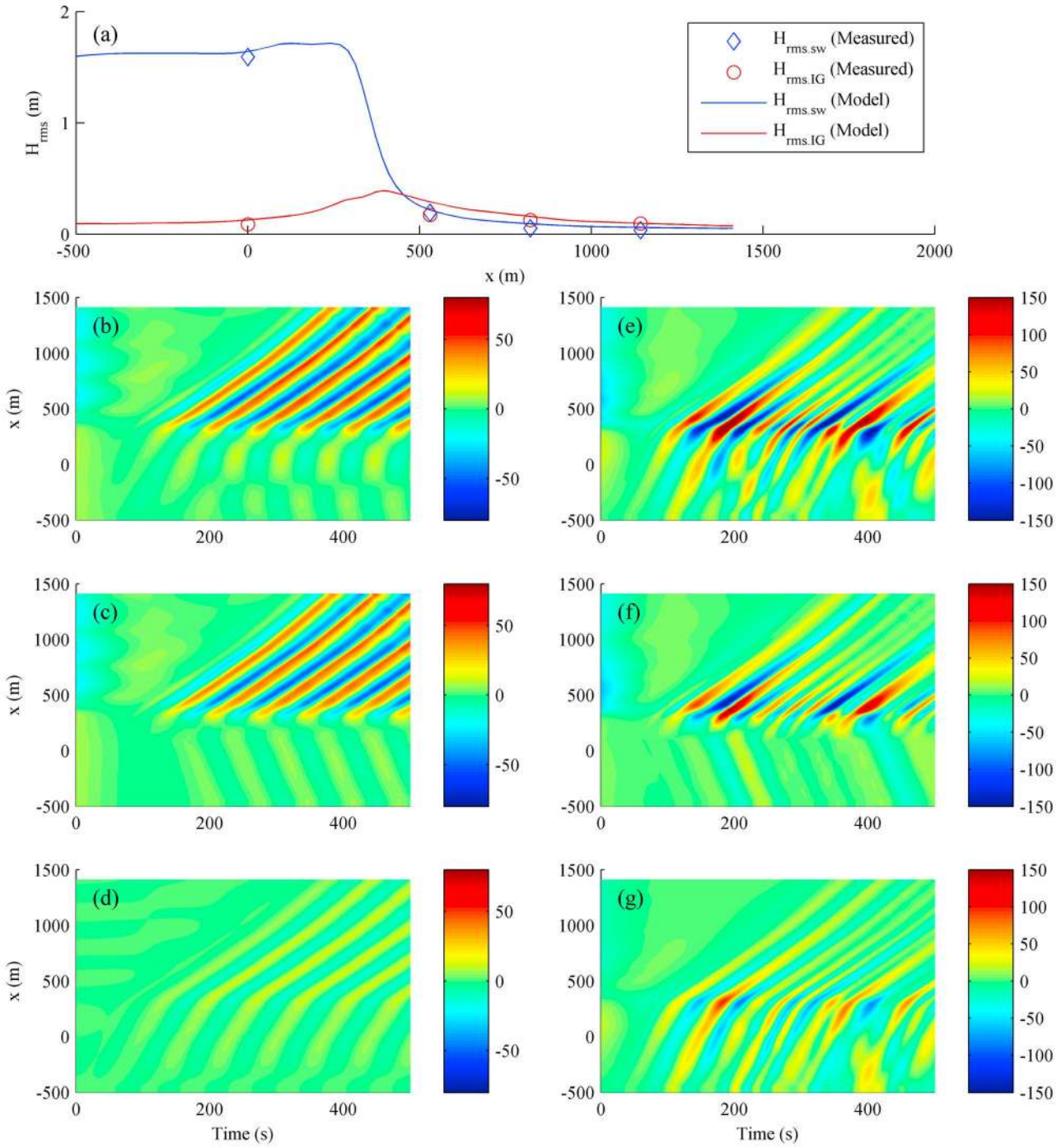

Figure 9. Plots of the offshore-generated and slope-generated infragravity wave elevations for bichromatic (Figures 9b–9d) and irregular (Figures 9e–9g) forcing for the swell event at 05:00, 16 June 2009. (a) Comparison of the modeled and observed short-wave and IG wave heights during the swell event (irregular wave case). (b, e) Contribution to the infragravity wave height of the full model solution with both bound and surf zone–generated waves included in the model, (c, f) surf zone–generated wave contribution (no bound wave generation), and (d, g) the bound wave contribution (no surf zone generation).

(Figure 9e) reveals a complex pattern of offshore IG waves, which is due to the interaction between the incident bound waves and the seaward propagating surf zone (breakpoint) generated IG waves. When the bound wave forcing is turned off in the offshore region (Figure 9f), only seaward directed waves are observed offshore of the surf zone, along with shoreward propagating IG waves out of the surf zone, yet the IG wave heights on the reef are effectively the same as the full forcing case (Table 4), i.e., the inclusion of the incident bound waves do not make an important contribution to the IG wave heights observed on the reef. Likewise for the case with the generation of the surf zone (breakpoint) forcing

Table 4. Root-Mean-Square Infragravity Wave Heights $H_{rms,IG}$ Predicted by XBeach

	Bichromatic Waves (cm)		Irregular Waves (cm)	
Model Case	C1	C3	C1	C3
Full case	2.0	9.5	13.0	29.0
Surf zone forcing only	1.4	9.0	6.3	29.0
No surf zone forcing	1.1	2.3	9.8	9.8

turned off (Figure 9g), the IG wave heights on the reef are reduced by ~70% from the full forcing case (Table 4).

[33] Using the results for the irregular wave case (16 June 5:00), we conducted the same lagged cross-correlation analysis between the incident short-wave envelope $|A(t)|$ at C1 with the IG wave time series η_{IG} at all locations across the model domain (Figure 10), which facilitates comparison with the field results in Figure 5a. A similar transition occurs in the surf zone region between C1 and C3, with a dominant negative correlation in the offshore region, characteristic of the incident bound wave, and then a strong positive correlation across the reef and lagoon generated by the breakpoint mechanism. As the bound wave approaches the surf zone, a region of elevated surface elevation (positive correlation) develops in front of the wave group as a result of "dynamic setup," thus consistent with the laboratory observations by *Baldock* [2006] (see Figure 5 in that paper and associated discussion). A negative correlation is also observed propagating seaward out of the surf zone (thus of opposite sign to the shoreward propagating positive signal), which are both characteristics of the breakpoint forcing mechanism [*Symonds et al.*, 1982; *Baldock and Huntley*, 2002]. This negative lag at C1 at time ~+80 s is also visible in the field results (refer to the star in Figure 5a). Overall, these correlation patterns are consistent with laboratory observations and numerical modeling results of IG wave generation on steep ~1:10 "beaches" [*Baldock*, 2006; *Lara et al.*, 2011; *Baldock*, 2012], but contrast with the propagation of a dominant negative correlation all the way to shore shown by *Janssen et al.* [2003] for a mild-slope (~1:70) beach study that emphasized the important role of shoaling bound waves in this mild-slope regime.

[34] The fate of the bound wave through a surf zone is still the subject of debate (e.g., as summarized recently in *Baldock* [2012]) with different opinions on whether these waves may be "released" or dissipated with the short-wave breaking. In this study, it appears that the sudden (and strong) dissipation of the incident short waves result in most of the bound waves associated with the incident wave groups being dissipated coincident with the short wave breaking through the surf zone. Without additional field instrumentation within the surf zone, this cannot be verified with certainty from the observational component.

4.3. Propagation of IG Waves

[35] The IG waves in this study propagated shoreward across the reef and lagoon with lags in the cross-correlation analysis agreeing with those expected from the linear shallow water wave speed (Figures 5a and 5b). Combined with the observation of linear ramps in the cross-spectral phase spectra

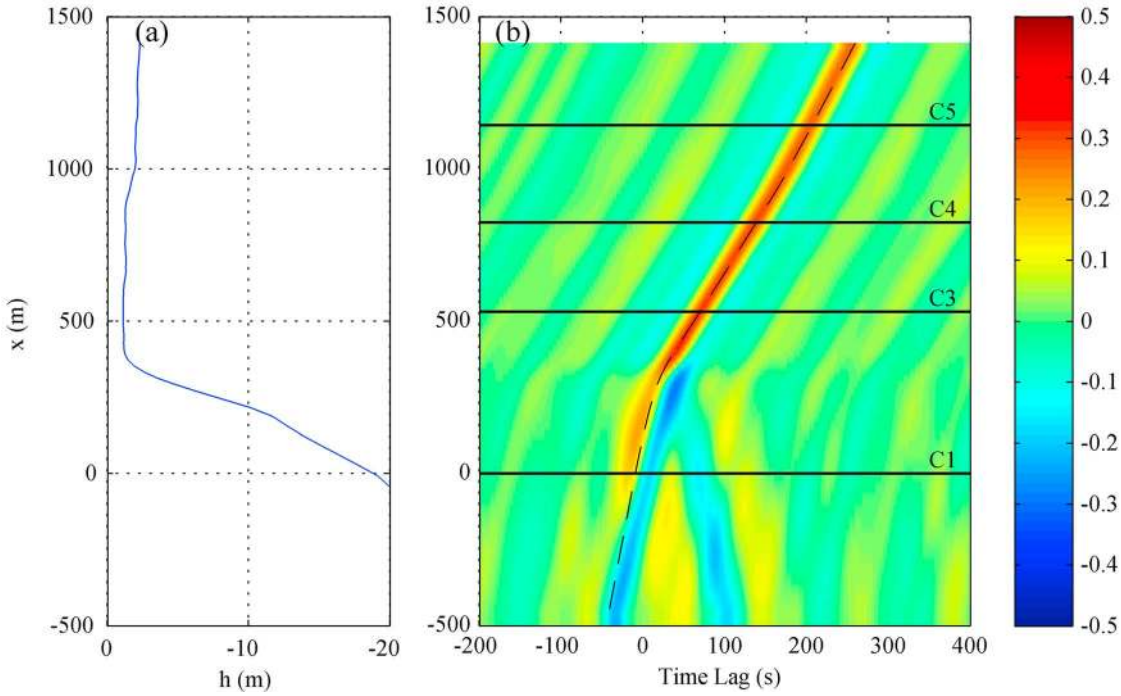

Figure 10. (a) The Ningaloo Reef bathymetry used in the XBeach model. (b) Cross correlation of the amplitude of the short-wave envelope $|A(t)|$ at C1 with the shoreward IG wave time series η_{IG} at each instrument location with the results from XBeach for the irregular wave case forced by the swell conditions of 16 June, 05:00. The dashed line denotes the theoretical linear shallow water speed trajectory obtained by integration of the bathymetry profile.

and the low reflection coefficient values throughout the reef and lagoon ($R^2_{IG} < 0.25$–0.5), this indicates a dominance of shoreward propagating progressive IG motions throughout the reef, which is in contrast to the more typical cross-shore standing wave patterns observed on beaches [e.g., *Masselink*, 1995]. These results are also different from observations made over a fringing reef at Guam [*Péquignet et al.*, 2009] that showed the strong formation of an IG standing wave across the reef during a period where the water level was raised over the reef during a tropical storm. In the Guam case, this implies the IG waves were reflected from the mainland coast with far greater energy preserved, perhaps in part due to that reef being much narrower than Ningaloo (by a factor of ~4) and partly due to the reduced influence of bottom friction that resulted from the increased water level (wave setup) during the tropical storm.

[36] From these dynamics we can thus construct a conceptual model of the IG motions on the reef, where waves generated in the surf zone first propagate shoreward as damped progressive waves. Bottom friction reduces the height of the IG waves such that limited IG energy remains in the lagoon. At the lagoon site (C5), reflection coefficients were somewhat higher ($R^2_{IG} \sim 0.5$) than at the seaward reef station, suggesting that some shoreline reflection of IG wave energy was present, although values are far less than 1 implying that some shoreline dissipation also occurs. These results are consistent with swash observations from low-sloping beaches (~1:50), which have highlighted that shoreline dissipation can be significant [e.g., *Ruessink et al.*, 1998; *Ruggiero et al.*, 2004] and that shoreline IG reflection coefficients can also be less than one. Significant shoreline dissipation has also been observed on steep beaches under energetic IG conditions [e.g., *Senechal et al.*, 2011], albeit for incident waves much greater than those incident to these reef-protected beaches. For the section of reef studied, the sandy beach slopes are locally variable, ranging from 1:20 to much greater than 1:50, so some shoreline dissipation of IG wave energy (and hence reflection coefficients near the shore being much less than 1) would not be unexpected.

[37] The remaining seaward reflected IG waves emanating from the shoreline (which are already very small in height) then decay further due to bottom friction, such that virtually no seaward directed IG wave energy remains on the seaward margins of the reef (i.e., sites C3 and C4). As a result, the combined IG motions on the reef flat are dominantly shoreward progressive, which can also explain the lack of any significant seaward propagation of IG waves from the shoreline in the correlation analysis (Figure 5); a response that differs from analogous observations on sandy beaches [e.g., *Guza and Thornton*, 1985] where coherent shoreline reflections are often observed.

4.4. Energy Dissipation

[38] There was a substantial (2 orders of magnitude) reduction (likely dominated by wave breaking) in the short-wave energy fluxes for the fore reef and reef crest region between C1 and C3. As observed in other reef studies, some short-wave energy (limited by the tidal depth over the reef) propagated toward the shore out of the surf zone [*Hardy and Young*, 1996; *Nelson*, 1994; *Lowe et al.*, 2005; *Péquignet et al.*, 2011]; however, these residual short waves decayed fairly rapidly across the reef flat by bottom friction. In contrast, this study has demonstrated for the first time, that despite the shoreward propagating IG waves experiencing substantial frictional dissipation that limited the amount of energy reaching the shoreline, the rate of IG wave decay was considerably smaller than for the short waves. As a result, the total wave energy fluxes were initially partitioned roughly equally between short waves and IG waves near the reef crest (Figures 6d and 6e), but eventually the IG waves overwhelmingly dominated toward the lagoon (Figures 6j and 6k).

[39] Rates of frictional wave dissipation of short waves over reefs have been the focus of several other studies, with the observed (short-wave) wave friction coefficients f_w being much larger (typically ~0.2–0.3 or more) [e.g., *Gerritsen*, 1980; *Lowe et al.*, 2005; *Péquignet et al.*, 2011], than the friction coefficients associated with mean currents over reefs (typically, 0.02–0.05) [*Hench et al.*, 2008; *Lowe et al.*, 2008, 2009]. This is due to the strong dependency of the friction coefficients on the ratio of the wave orbital excursion (effectively infinite for a mean current) and a hydraulic roughness length scale associated with the rugosity of the reef [*Nielsen*, 1992]. Nevertheless, although the value of $f_c = 0.06$ associated with the dissipation of the IG waves in this study is much smaller than reported values of f_w for reefs, it is still large enough to significantly reduce the IG waves across the wide reef flat.

[40] This high frictional dissipation of IG waves would also occur in the surf zone region between C1 and C3, resulting in a more complicated energy partitioning between generation and dissipation. Therefore, the fact that the shoreward IG wave energy fluxes F^+_{IG} tend to be comparable in magnitude on the fore reef at C1 (associated with a bound wave prior to short-wave breaking) and at C3 on the reef flat (associated with the resulting free wave shoreward of the surf zone), does not imply the shoaling bound wave generation mechanism is important, which could be incorrectly assumed if the strong IG wave dissipation in the surf zone was neglected. Furthermore, on the fore reef (C1) prior to short-wave breaking, the net IG energy fluxes (seaward minus shoreward) tend to cancel (Figure 6b) as result of the strong seaward directed IG wave fluxes F^-_{IG} generated in the surf zone by the breakpoint forcing mechanism (Figure 9). Ultimately, the net shoreward energy fluxes are much greater on the reef at C3 (despite frictional losses in the surf zone) due to the energy provided by breakpoint forcing.

[41] The results also showed that the friction coefficients f_c associated with the IG waves were weakly affected by changes in the tidal elevation over the reef. This trend can be explained by the known decrease in friction coefficients (relating bottom stresses to the depth-averaged flow) with increasing water depth per open channel flow theory. Given the long period of the IG motions (order 100 s), the vertical flow structure would be expected to follow that of an effectively unidirectional flow. While the flow structure near the bed of coral reefs having large bottom roughness and associated form drag is best described by canopy flow theory within the canopy layer itself (i.e., below the height of the coral roughness) [e.g., see *Rosman and Hench*, 2011], unidirectional flow in the water column above submerged canopies have been shown to tend

toward a logarithmic velocity profile characteristic of rough-wall turbulent boundary layer flows [see *Nepf and Vivoni*, 2000]. For this reef, the dominant plate Acropora (height typically 20–30 cm) only occupies 10–20% of the water depth (Figure 1c) and if we assume a logarithmic boundary layer profile on the reef flat, we can integrate over the depth h to obtain a relationship between the friction coefficient f_c (defined based on the depth-averaged flow) and a hydraulic roughness length z_0 [e.g., *Burchard et al.*, 2011]

$$f_c = \left[\frac{\kappa}{\left(1+\frac{z_0}{h}\right)\ln\left(\frac{h}{z_0}+1\right)-1}\right]^2. \quad (8)$$

[42] Thus, for a fixed physical roughness defined by z_0, equation (8) predicts that f_c will decrease with increasing water depth, with this dependency being much stronger in very shallow water columns (i.e., when $z_0/h \gtrsim 0.001$). Figure 8b shows the relationship predicted by equation (8) with $z_0 = 0.15$ m, which follows a very similar trend to the data.

[43] In contrast to some recent studies on beaches [*Thomson et al.*, 2006; *Henderson et al.*, 2006], rates of nonlinear energy transfer N_{IG} from the IG waves on the reef flat were found to be minimal in comparison to the high rates of frictional dissipation D_{IG}. In general, some weak nonlinear interactions were shown to transfer energy from the short-wave frequency band to the IG frequency band on the reef flat, i.e., at times these nonlinear transfers were a weak source of energy gain to the IG band. This weak transfer is likely due to the limited presence of short waves on the reef flat that continue to be dissipated by bottom friction as they propagate across the reef. We emphasize that the importance of dissipation to nonlinear energy transfer will be much different in the surf zone region where no direct field measurements were made, i.e., high rates of energy transfer from the short waves N_{IG} by definition must be much more important than local rates of dissipation D_{IG} to account for the IG wave motions on the reef.

[44] Finally, the results showed that the height of IG waves $H_{rms,IG}$ on the reef were strongly dependent on the tidal elevation (Figures 4b and 4c), with a general trend of decreasing $H_{rms,IG}$ as the total water depth h (measured at C3) decreased, to a point where $H_{rms,IG}$ was effectively zero for depths <1 m. This trend can be explained by the modulation of rates of bottom friction dissipation D_{IG} resulting from two mechanisms: 1) the direct dependency of $D_{IG} \sim h^{-3/2}$ per equation (5) and 2) the response of f_c to the water depth per equation (8) (Figure 8b). Conversely, the results in Figures 4b and 4c suggest a gradual leveling off of the $H_{rms,IG}/H_{rms,sw}$ versus depth curves for larger water depth ($h > 2$ m). This is likely due to the efficiency of the breakpoint mechanism decreasing as the water depth over the reef increases (and hence rates of depth-limited short-wave breaking decreasing), which results in a reduction of wave forces generated inside the surf zone.

5. Summary and Conclusions

[45] A field study was conducted at Sandy Bay in Ningaloo Reef (Western Australia) to quantify the dynamics of IG wave motion across this fringing reef during a range of incident short-wave (swell) conditions. The short waves were dissipated rapidly by depth-limited breaking on the relatively steep (~1:20) fore-reef slope. Low-frequency (infragravity) waves were generated during the short-wave breaking processes, with both the field results and supplemental numerical modeling results emphasizing the importance of the breakpoint forcing mechanism to the IG waves observed on the reef. The results are consistent with theory suggesting that the breakpoint forcing mechanism becomes more efficient to IG wave generation (compared to shoaling bound waves) in this steep slope regime.

[46] The infragravity waves generated inside the surf zone propagated shoreward across the reef and lagoon as damped progressive waves. Over the reef flat, the IG wave field energy losses were primarily due to bottom friction rather than nonlinear energy transfers, which differs from recent observations on sandy beaches. While rates of bottom friction dissipation experienced by the IG waves (equivalent to $f_c \sim 0.06$) were much higher than those expected for a sandy bed, they were still not large enough to completely damp out the IG waves reaching the shoreline (i.e., IG wave heights in the lagoon were still ~30% of the values at the reef crest, on average). Moreover, our results indicate that bottom friction has a much greater effect on damping the short waves compared to the IG waves, consistent with expected differences in the magnitude of short-period wave (f_w) and low-frequency current (f_c) friction coefficients observed in nearshore environments, including reefs. As a consequence, the IG waves play an increasingly important role across the reef, and ultimately dominate inside the lagoon. While there was some evidence of weak shoreline reflection of the remaining lagoon IG wave energy, these seaward propagating IG waves would experience additional high rates of frictional damping over this wide and shallow reef. Thus, with the seaward flux contribution minimal to the overall IG wave motions on the reef, progressive shoreward propagating IG waves dominate throughout the reef system.

[47] The results also revealed a strong depth dependency of the IG wave heights on the water level over the reef (as modulated by the tide), with larger heights at greater depth. This is mostly due to strong dependency of IG frictional dissipation rates with the total water depth over the reef, due to the smaller influence of frictional dissipation on the total wave energy flux as well as the reduction of f_c that both occur in a deeper water column. As a result, this present study demonstrates that the height of IG waves on reefs is highly sensitive to changes in the mean water level over the reef, independent of IG wave resonance documented by *Péquignet et al.* [2009], which suggests that the capacity of reefs to protect shorelines from incident wave energy may be further reduced by a future rise in mean sea level.

[48] **Acknowledgments.** We are grateful to Jim Falter and Nick Mortimer for assistance with the instrument deployment and recovery and thank three anonymous reviewers and Gerben Ruessink for providing comments that substantially improved the manuscript. Funding for this project was provided by an Australian Research Council Discovery Grant (DP0770094) and Australian Research Council Future Fellowship (FT110100201) to R.J.L. and a CSIRO Flagship Collaboration Fund award to R.J.L., G.S., and A.V.D. Additional funding to A.V.D. and A.W.P. was provided by the Deltares Strategic Research Project 1202362 (System Tools). A.W.P. acknowledges funding provided by the European Commission Erasmus Mundus Program.

References

Atkinson, M. J., and J. L. Falter (2003), Coral reefs, in *Biogeochemistry of Marine Systems*, edited by K. P. Black and G. B. Shimmield, pp. 40–64, CRC Press, Boca Raton, Fla.

Baldock, T. E. (2006), Long wave generation by the shoaling and breaking of transient wave groups on a beach, *Proc. R. Soc. A*, *462*(2070), 1853–1876.

Baldock, T. E. (2012), Dissipation of incident forced long waves in the surf zone—Implications for the concept of "bound" wave release at short wave breaking, *Coastal Eng.*, *60*, 276–285, doi:10.1016/j.coastaleng.2011.11.002.

Baldock, T. E., and D. A. Huntley (2002), Long–wave forcing by the breaking of random gravity waves on a beach, *Proc. R. Soc. London, Ser. A*, *458*(2025), 2177–2201.

Baldock, T. E., D. A. Huntley, P. A. D. Bird, T. O'Hare, and G. N. Bullock (2000), Breakpoint generated surf beat induced by bichromatic wave groups, *Coastal Eng.*, *39*, 213–242, doi:10.1016/S0378-3839(99)00061-7.

Battjes, J. A., H. J. Bakkenes, T. T. Janssen, and A. R. van Dongeren (2004), Shoaling of subharmonic gravity waves, *J. Geophys. Res.*, *109*, C02009, doi:10.1029/2003JC001863.

Bendat, J. S., and A. G. Piersol (1986), *Random Data, Analysis and Measurement*, John Wiley, New York.

Brander, R. W., P. S. Kench, and D. Hart (2004), Spatial and temporal variations in wave characteristics across a reef platform, Warraber Island, Torres Strait, Australia, *Mar. Geol.*, *207*(1–4), 169–184, doi:10.1016/j.margeo.2004.03.014.

Burchard, H., R. D. Hetland, E. Schulz, and H. M. Schuttelaars (2011), Drivers of residual estuarine circulation in tidally energetic estuaries: Straight and irrotational channels with parabolic cross section, *J. Phys. Oceanogr.*, *41*(3), 548–570, doi:10.1175/2010JPO4453.1.

Dean, R. G., and R. A. Dalrymple (1991), *Water Wave Mechanics for Engineers and Scientists*, *Adv. Ser. Ocean Eng.*, vol. 2, World Sci., Singapore.

Demirbilek, Z., O. G. Nwogu, and D. L. Ward (2007), Laboratory study of wind effect on runup over fringing reef, report 1: Data report, *Tech. Rep. ERDC/CHL TR-07–4*, Coastal and Hydraul. Lab., Vicksburg, Miss.

Dollar, S. J. (1982), Wave stress and coral community structure in Hawaii, *Coral Reefs*, *1*, 71–81, doi:10.1007/BF00301688.

Elgar, S., and R. T. Guza (1985), Observations of bispectra of shoaling surface gravity waves, *J. Fluid Mech.*, *161*, 425–448, doi:10.1017/S0022112085003007.

Elgar, S., T. H. Herbers, M. Okihiro, J. Oltman-Shay, and R. T. Guza (1992), Observations of infragravity waves, *J. Geophys. Res.*, *97*, 15,573–15,577, doi:10.1029/92JC01316.

Foda, M. A., and C. C. Mei (1981), Nonlinear excitation of long-trapped waves by a group of short swells, *J. Fluid Mech.*, *111*, 319–345, doi:10.1017/S0022112081002401.

Gerritsen, F. (1980), Wave attenuation and wave set-up on a coastal reef, in *Proceedings of the 17th International Conference on Coastal Engineering*, 444–461, Am. Soc. of Civ. Eng., Reston, Va.

Gourlay, M. R. (1994), Wave transformation on a coral reef, *Coastal Eng.*, *23*, 17–42, doi:10.1016/0378-3839(94)90013-2.

Guza, R. T., and E. B. Thornton (1985), Observations of surf beat, *J. Geophys. Res.*, *90*(C2), 3161–3172, doi:10.1029/JC090iC02p03161.

Guza, R. T., E. B. Thornton, and R. A. Holman (1984), Swash on steep and shallow beaches, in *Proceedings of the 19th International Conference on Coastal Engineering, Houston*, pp. 708–723, Am. Soc. of Civ. Eng., Reston, Va.

Hardy, T. A., and I. R. Young (1996), Field study of wave attenuation on an offshore coral reef, *J. Geophys. Res.*, *101*(C6), 14,311–14,326, doi:10.1029/96JC00202.

Hench, J. L., J. J. Leichter, and S. G. Monismith (2008), Episodic circulation and exchange in a wave-driven coral reef and lagoon system, *Limnol. Oceanogr.*, *53*, 2681–2694, doi:10.4319/lo.2008.53.6.2681.

Henderson, S. M., and A. J. Bowen (2002), Observations of surf beat forcing and dissipation, *J. Geophys. Res.*, *107*(C11), 3193, doi:10.1029/2000JC000498.

Henderson, S. M., R. T. Guza, S. Elgar, T. H. C. Herbers, and A. J. Bowen (2006), Nonlinear generation and loss of infragravity wave energy, *J. Geophys. Res.*, *111*, C12007, doi:10.1029/2006JC003539.

Herbers, T. H. C., and M. C. Burton (1997), Nonlinear shoaling of directionally spread waves on a beach, *J. Geophys. Res.*, *102*(C9), 21,101–21,114, doi:10.1029/97JC01581.

Herbers, T. H. C., S. Elgar, R. T. Guza, and W. C. O'Reilly (1995), Infragravity-frequency (0.005–0.05 Hz) motions on the shelf. Part II: Free waves, *J. Phys. Oceanogr.*, *25*(6), 1063–1079, doi:10.1175/1520-0485(1995)025<1063:IFHMOT>2.0.CO;2.

Hoeke, R., C. Storlazzi, and P. Ridd (2011), Hydrodynamics of a bathymetrically complex fringing coral reef embayment: Wave climate, in situ observations, and wave prediction, *J. Geophys. Res.*, *116*, C04018, doi:10.1029/2010JC006170.

Huntley, D. A., R. T. Guza, and E. B. Thornton (1981), Field observations of surf beat: 1. Progressive edge waves, *J. Geophys. Res.*, *86*(C7), 6451–6466, doi:10.1029/JC086iC07p06451.

Janssen, T. T., J. A. Battjes, and A. R. Van Dongeren (2003), Long waves induced by short-wave groups over a sloping bottom, *J. Geophys. Res.*, *108*(C8), 3252, doi:10.1029/2002JC001515.

Kim, Y. C., and E. J. Powers (1979), Digital bispectral analysis and its applications to nonlinear wave interactions, *IEEE Trans. Plasma Sci.*, *7*, 120–131, doi:10.1109/TPS.1979.4317207.

Kraines, S. B., A. Suzuki, T. Yanagi, M. Isobe, X. Y. Guo, and H. Komiyama (1999), Rapid water exchange between the lagoon and the open ocean at Majuro Atoll due to wind, waves, and tide, *J. Geophys. Res.*, *104*, 15,635–15,653, doi:10.1029/1999JC900065.

Kraines, S. B., M. Isobe, and H. Komiyama (2001), Seasonal variations in the exchange of water and water-borne particles at Majuro Atoll, the Republic of the Marshall Islands, *Coral Reefs*, *20*, 330–340, doi:10.1007/s00338-001-0191-8.

Kunkel, C. M., R. W. Hallberg, and M. Oppenheimer (2006), Coral reefs reduce tsunami impact in model simulations, *Geophys. Res. Lett.*, *33*(23), L23612, doi:10.1029/2006GL027892.

Lara, J. L., A. Ruju, and I. J. Losada (2011), Reynolds averaged Navier–Stokes modelling of long waves induced by a transient wave group on a beach, *Proc. R. Soc. A.*, *467*, 1215–1242.

List, J. (1992), A model for the generation of two-dimensional surf beat, *J. Geophys. Res.*, *97*(C4), 5623–5635, doi:10.1029/91JC03147.

Longuet-Higgins, M. S., and R. W. Stewart (1962), Radiation stresses and mass transport in surface gravity waves and application to surf beats, *J. Fluid Mech.*, *13*, 481–504, doi:10.1017/S0022112062000877.

Lowe, R. J., J. L. Falter, M. D. Bandet, G. Pawlak, M. J. Atkinson, S. G. Monismith, and J. R. Koseff (2005), Spectral wave dissipation over a barrier reef, *J. Geophys. Res.*, *110*, C04001, doi:10.1029/2004JC002711.

Lowe, R. J., U. Shavit, J. L. Falter, J. R. Koseff, and S. G. Monismith (2008), Modeling flow in coral communities with and without waves: A synthesis of porous media and canopy flow approaches, *Limnol. Oceanogr.*, *53*(6), 2668–2680, doi:10.4319/lo.2008.53.6.2668.

Lowe, R. J., J. L. Falter, S. G. Monismith, and M. J. Atkinson (2009), Wave-driven circulation of a coastal reef-lagoon system, *J. Phys. Oceanogr.*, *39*, 873–893, doi:10.1175/2008JPO3958.1.

Lowe, R. J., C. Hart, and C. B. Pattiaratchi (2010), Morphological constraints to wave-driven circulation in coastal reef-lagoon systems: A numerical study, *J. Geophys. Res.*, *115*, C09021, doi:10.1029/2009JC005753.

Lugo-Fernández, A., H. H. Roberts, W. J. Wiseman Jr., and B. L. Carter (1998), Water level and currents of tidal and infragravity periods at Tague Reef, St. Croix (USVI), *Coral Reefs*, *17*, 343–349, doi:10.1007/s003380050137.

Massel, S. R., and M. R. Gourlay (2000), On the modelling of wave breaking and set-up on coral reefs, *Coastal Eng.*, *39*(1), 1–27, doi:10.1016/S0378-3839(99)00052-6.

Masselink, G. (1995), Group bound long waves as a source of infragravity energy in the surf zone, *Cont. Shelf Res.*, *15*(13), 1525–1547, doi:10.1016/0278-4343(95)00037-2.

Monismith, S. G. (2007), Hydrodynamics of coral reefs, *Annu. Rev. Fluid Mech.*, *39*, 37–55, doi:10.1146/annurev.fluid.38.050304.092125.

Munk, W. H. (1949), Surf beat, *Eos Trans. AGU*, *30*, 849–854.

Munk, W. H., and M. C. Sargent (1948), Adjustment of Bikini Atoll to ocean waves, *Eos Trans. AGU*, *29*, 855–860.

Nakaza, E., and M. Hino (1991), Bore-like surf beat in a reef zone caused by wave groups of incident short period waves, *Fluid Dyn. Res.*, *7*(2), 89–100, doi:10.1016/0169-5983(91)90062-N.

Nelson, R. C. (1994), Depth limited design wave heights in very flat regions, *Coastal Eng.*, *23*(1–2), 43–59, doi:10.1016/0378-3839(94)90014-0.

Nepf, H. M., and E. R. Vivoni (2000), Flow structure in depth-limited, vegetated flow, *J. Geophys. Res.*, *105*(C12), 28,547–28,557, doi:10.1029/2000JC900145.

Nielsen, P. (1992), *Coastal Bottom Boundary Layers and Sediment Transport*, *Adv. Ser. Ocean Eng.*, vol. 4, World Sci., Singapore.

Nwogu, O., and Z. Demirbilek (2010), Infragravity wave motions and runup over shallow fringing reefs, *J. Waterw. Port Coastal Ocean Eng.*, *136*, 295–305, doi:10.1061/(ASCE)WW.1943-5460.0000050.

Péquignet, A. C. N., J. M. Becker, M. A. Merrifield, and J. Aucan (2009), Forcing of resonant modes on a fringing reef during tropical storm Man-Yi, *Geophys. Res. Lett.*, *36*, L03607, doi:10.1029/2008GL036259.

Péquignet, A. C. N., J. M. Becker, M. A. Merrifield, and S. J. Boc (2011), The dissipation of wind wave energy across a fringing reef at Ipan, Guam, *Coral Reefs*, *30*, suppl. 1, 71–82, doi:10.1007/s00338-011-0719-5.

Roberts, C. M. (1997), Connectivity and management of Caribbean coral reefs, *Science*, *278*, 1454–1457, doi:10.1126/science.278.5342.1454.

Roelvink, D., and M. Stive (1989), Bar generating cross shore flow mechanisms on a beach, *J. Geophys. Res.*, *94*(C4), 4785–4800.

Roelvink, D., A. Reniers, A. van Dongeren, J. van Thiel de Vries, R. McCall, and J. Lescinski (2009), Modelling storm impacts on beaches, dunes and barrier islands, *Coastal Eng.*, *56*, 1133–1152, doi:10.1016/j.coastaleng.2009.08.006.

Roelvink, J. A., and A. J. H. M. Reniers (2012), *A Guide to Modelling Coastal Morphology*, World Sci., Singapore.

Rosman, J. H., and J. L. Hench (2011), A framework for understanding drag parameterizations for coral reefs, *J. Geophys. Res.*, *116*, C08025, doi:10.1029/2010JC006892.

Ruessink, B. G. (1998), Bound and free infragravity waves in the nearshore zone under breaking and nonbreaking conditions, *J. Geophys. Res.*, *103*(C6), 12,795–12,805, doi:10.1029/98JC00893.

Ruessink, B. G., M. G. Kleinhans, and P. G. L. van den Beukel (1998), Observations of swash under highly dissipative conditions, *J. Geophys. Res.*, *103*(C2), 3111–3118, doi:10.1029/97JC02791.

Ruggiero, P., R. A. Holman, and R. A. Beach (2004), Wave run-up on a high-energy dissipative beach, *J. Geophys. Res.*, *109*, C06025, doi:10.1029/2003JC002160.

Sanderson, P. G. (2000), A comparison of reef-protected environments in Western Australia: The central west and Ningaloo coasts, *Earth Surf. Processes Landforms*, *25*(4), 397–419, doi:10.1002/(SICI)1096-9837(200004)25:4<397::AID-ESP62>3.0.CO;2-9.

Schäffer, H. A., and I. A. Svendsen (1988), Surf beat generation on a mild slope, in *Coastal Engineering 1988*, pp. 1058–1072, Am. Soc. of Civ. Eng., Reston, Va.

Senechal, N., G. Coco, K. R. Bryan, and R. A. Holman (2011), Wave runup during extreme storm conditions, *J. Geophys. Res.*, *116*, C07032, doi:10.1029/2010JC006819.

Sheremet, A., R. T. Guza, S. Elgar, and T. H. C. Herbers (2002), Observations of nearshore infragravity waves: Seaward and shoreward propagating components, *J. Geophys. Res.*, *107*(C8), 3095, doi:10.1029/2001JC000970.

Sheremet, A., J. M. Kaihatu, S. F. Su, E. R. Smith, and J. M. Smith (2011), Modeling of nonlinear wave propagation over fringing reefs, *Coastal Eng.*, *58*(12), 1125–1137, doi:10.1016/j.coastaleng.2011.06.007.

Storlazzi, C. D., A. S. Ogston, M. H. Bothner, M. E. Field, and M. K. Presto (2004), Wave- and tidally driven flow and sediment flux across a fringing coral reef: Southern Molokai, Hawaii, *Cont. Shelf Res.*, *24*(12), 1397–1419, doi:10.1016/j.csr.2004.02.010.

Suhayda, J. N. (1974), Standing waves on beaches, *J. Geophys. Res.*, *79*, 3065–3071, doi:10.1029/JC079i021p03065.

Symonds, G., D. A. Huntley, and A. J. Bowen (1982), Two-dimensional surf beat: Long wave generation by a time-varying breakpoint, *J. Geophys. Res.*, *87*(C1), 492–498, doi:10.1029/JC087iC01p00492.

Taebi, S., R. J. Lowe, C. B. Pattiaratchi, G. N. Ivey, G. Symonds, and R. Brinkman (2011), Nearshore circulation in a tropical fringing reef system, *J. Geophys. Res.*, *116*, C02016, doi:10.1029/2010JC006439.

Thomson, J., S. Elgar, B. Raubenheimer, T. H. C. Herbers, and R. T. Guza (2006), Tidal modulation of infragravity waves via nonlinear energy losses in the surfzone, *Geophys. Res. Lett.*, *33*, L05601, doi:10.1029/2005GL025514.

Tucker, M. J. (1950), Surf beats: Sea waves of 1 to 5 minute period, *Proc. R. Soc. London, Ser. A*, *202*, 565–573, doi:10.1098/rspa.1950.0120.

Van Dongeren, A., A. Reniers, J. Battjes, and I. Svendsen (2003), Numerical modeling of infragravity wave response during DELILAH, *J. Geophys. Res.*, *108*(C9), 3288, doi:10.1029/2002JC001332.

Van Dongeren, A., J. Battjes, T. Janssen, J. van Noorloos, K. Steenhauer, G. Steenbergen, and A. Reniers (2007), Shoaling and shoreline dissipation of low-frequency waves, *J. Geophys. Res.*, *112*, C02011, doi:10.1029/2006JC003701.

Van Thiel de Vries, J. S. M. (2009), Dune erosion during storm surges, PhD thesis, Tech. Univ. of Delft, Delft, Netherlands.

Williams, J. J., A. R. de Alegría-Arzaburu, R. T. McCall, and A. Van Dongeren (2012), Modelling gravel barrier profile response to combined waves and tides using XBeach: Laboratory and field results, *Coastal Eng.*, *63*, 62–80.

Wyatt, A. S. J., R. J. Lowe, S. Humphries, and A. M. Waite (2010), Particulate nutrient fluxes over a fringing coral reef: Relevant scales of phytoplankton production and mechanisms of supply, *Mar. Ecol. Prog. Ser.*, *405*, 113–130, doi:10.3354/meps08508.

Yahel, G., A. F. Post, K. Fabricius, D. Marie, D. Vaulot, and A. Genin (1998), Phytoplankton distribution and grazing near coral reefs, *Limnol. Oceanogr.*, *43*, 551–563, doi:10.4319/lo.1998.43.4.0551.

Zhang, Z., R. J. Lowe, J. Falter, and G. Ivey (2011), A numerical model of wave- and current-driven nutrient uptake by coral reef communities, *Ecol. Modell.*, *222*, 1456–1470, doi:10.1016/j.ecolmodel.2011.01.014.